AIMS Materials Science, 2(4): 425-447.
DOI: 10.3934/matersci.2015.4.425
Received date 15 August 2015,
Accepted date 6 November 2015,
Published date 12 November 2015

http://www.aimspress.com/

Research article

Effect of blasts on subject-specific computational models of skin and bone sections at various locations on the human body

Arnab Chanda [1], Rebecca Graeter [2], and Vinu Unnikrishnan [1,*]

[1] Department of Aerospace Engineering and Mechanics, The University of Alabama, Tuscaloosa AL 35487, USA
[2] School of Chemical Engineering, Mississipi State University, USA

*** Correspondence:** E-mail: vunnikrishnan@eng.ua.edu; Tel: +1-205-348-5193.

Abstract: Blast injuries are very common among soldiers deployed in politically unstable regions such as Afghanistan and Iraq, and also in a battle field anywhere in the world. Understanding the mechanics of interaction of blasts with the skin and bone at various parts of the human body is the key to designing effective personal protective equipment (PPE's) which can mitigate blast impacts. In the current work, subject-specific 3D computational models of the skin (with the three layers namely the epidermis, dermis and the hypodermis (muscles)) and bone sections from various parts of the human body (such as the elbow, finger, wrist, cheek bone, forehead, shin etc.) have been developed to study the effect of blast loading. Non-linear material properties have been adopted for the skin and stress impulses at the different skin layers and bone sections are estimated. To date, such an extensive study on the effect of blast loading on the human skin and bone has not been attempted. The results of this study would be indispensable for medical practitioners to understand the effect of blast trauma and plan effective post-traumatic surgical strategies, and also for developing better PPE designs for the military in the future.

Keywords: blast; skin; bone; subject-specific; computational model

1. Introduction

Blast injuries are common in a battlefield, and often, severe injuries with post-traumatic effects (such as the Traumatic Brain Injury (TBI)) are observed in such blast situations, than death. To date,

the personal protection equipment (PPE's) designed by the U.S. military are not sufficient for blast resistance [1]. Also the biomechanics of blast injury and trauma is poorly understood by doctors and medical practitioners [2].

A blast wave is physically a sudden expanding volume of compressed gas, which may cause injury to the human body in numerous ways and in varying degrees of harm [3,4]. Blast injuries can be categorized into four major types: primary, secondary, tertiary, and mutilating. Primary blast injury is caused by a blast wave striking the body and transmitting energy directly into the body. Secondary blast injury occurs by debris propelled onto or into the body by the blast or its blast wave. The force with which a blast occurs is called its load. Blast loading can inflict enough stress on the body to cause it to be flung onto a structure where tertiary blast injury can occur. It can even cause a mutilating blast injury, or traumatic amputation of one or more of the body parts.

A blast wave consists of two parts namely positive and negative sections. A typical blast wave pressure profile (see Figure 1) in open air is characterized by the Friedlander wave equation [3,4]. The positive portion of the plot corresponds to a sudden rise in pressure, which dissipates within a short distance and time span. Right after the positive phase dissipates, a negative pressure phase (forming a vacuum type atmosphere) develops. The highest point of the blast pressure profile is called the blast overpressure (or peak).

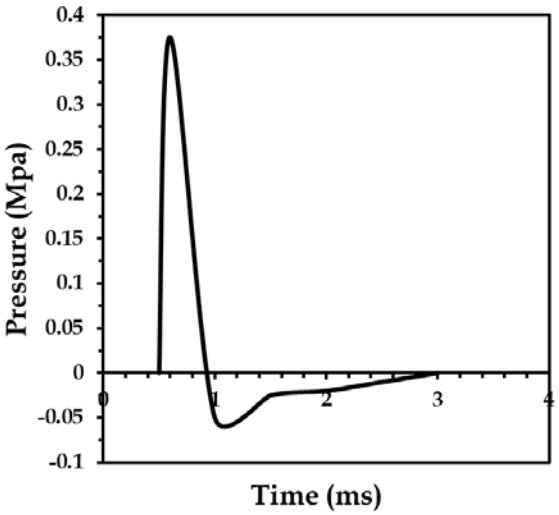

Figure 1. Air pressure plot of a blast scenario.

In literature, the effect of blasts on the human head has been studied extensively using experimental [5–10] and computational modelling [5–16] techniques. Mostly, experiments have been conducted on either live human subjects, cadavers, animal models or surrogates [1,16,17]. The major disadvantages associated with such experimental tests are: 1) Limited availability and high cost, 2) Ethical issues associated with testing on live human subjects, and 3) Drastic change in the material properties of human tissues with death in cadavers. A plethora of computational models to study the effect of blasts induced Traumatic Brain Injury (b-TBI) have been developed by Ganpule et al. [7,8,12–14] and others [1,2,5,9,11,15–18]. However, to date, a very few studies have focussed on blast induced injuries on the other parts of the human body. In fact, in literature, besides the head, body locations such as the elbow, wrist, face, foot etc. have been found to be highly vulnerable to

injuries occurring from blasts [2,4,17–25]. This warrants a detailed study on the mechanics of such whole body injuries, which would be an indispensable first step towards designing of blast resistant PPE's and body armours in the future.

Recently, the effect of blast loading on the human skeleton [26] and the effect of landmines on the lower extremity (the foot) [27] were studied numerically using Finite Element Method (FEM). High blast induced dynamic stresses were observed at the bones which may cause traumatic fractures. Based on this study, our current work aims to further investigate the mechanics of interaction of blasts with the various skin layers namely the epidermis, dermis, the hypodermis (or muscle), and also the bone section, at various locations of the human body, using novel subject-specific computational modelling techniques. Section 2 presents the various geometrical and FEM techniques adopted in our analyses. Section 3 discusses the various results followed by the conclusions in Section 4.

2. Materials and Methods

2.1. Geometrical modeling

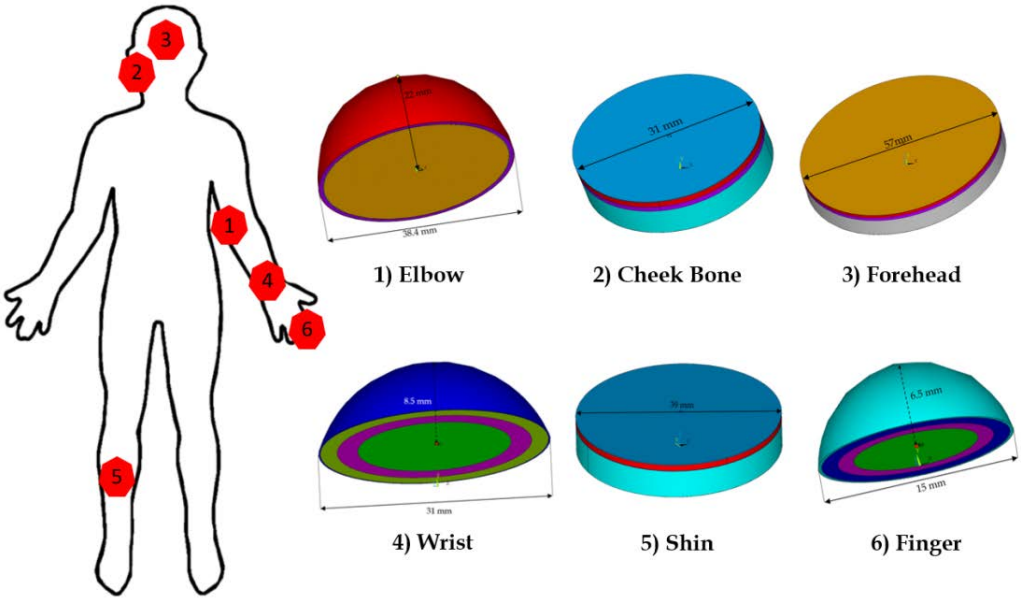

Figure 2. Subject-Specific geometrical models of skin and bone sections, based on anatomical locations on the human body.

For our study, skin and bone sections from six locations of the body namely the elbow, finger, wrist, cheek bone, forehead and shin, were chosen and modelled based on the knowledge of human anatomy [28] and eye estimation of three subjects (One Caucasian, and two Asians) [28,29] representing an average age group of 19–27 years. A 3D circular section with the various skin layers namely the epidermis, dermis, hypodermis (muscles), and bone were modelled in finite element software ANSYS. Locations such as the finger, elbow and the wrist which have a significant curvature were modelled as curved spherical surfaces, and the rest of the sections were modelled as flat cylindrical stacks of skin layers and bone, as shown in Figure 2. The thickness of the different

skin layers were chosen based on the extensive human skin thickness data available in literature [30–43].The approximate dimensions of the skin and bone section geometries used in our work are presented in Figure 2, and the thickness values adopted for different skin and bone section layers are listed in Table 1. It should be mentioned that the thickness for the bone is assumed only for a small section of the bone and not the entire bone.

Contact pairs were placed numerically to ensure contact between the various skin and bone section layers. The type of contact pair chosen was "bonded always", with negligible friction. The various constraints and loading conditions adopted for our study are discussed in the upcoming finite element modelling section 2.2.

Table 1. Subject and body location specific thicknesses of various skin and bone section layers adopted for developing the geometrical models.

Thickness (mm)	Elbow (*Curved*)	Finger (*Curved*)	Wrist (*Curved*)	Cheek bone (*Flat*)	Forehead (*flat*)	Shin (*flat*)
Subject 1 (Caucasian)						
Epidermis	0.09	0.22	0.14	0.13	0.11	0.14
Dermis	1.23	0.98	1.15	1.12	0.85	0.97
Hypodermis (Muscles)	0.11	1.22	1.56	1.17	0.08	0.08
Bone section	6.25 (*Radius*)	4.78 (*Radius*)	8.77 (*Radius*)	5.45	5.12	5.30
Subject 2 (Asian)						
Epidermis	0.08	0.19	0.1	0.09	0.09	0.09
Dermis	1.03	0.93	1.0	1.07	0.78	0.92
Hypodermis (Muscles)	0.08	1.2	1.53	1.0	0.07	0.07
Bone section	5.66 (*Radius*)	3.28 (*Radius*)	8.48 (*Radius*)	5.0	5.25	4.80
Subject 3 (Asian)						
Epidermis	0.13	0.25	0.15	0.16	0.11	0.13
Dermis	1.20	1.23	1.45	1.27	0.92	0.96
Hypodermis (Muscles)	0.12	1.16	1.74	1.10	0.08	0.07
Bone section	5.45 (*Radius*)	3.65 (*Radius*)	8.20 (*Radius*)	5.68	5.94	4.5

2.2. Finite element modeling

Development of a finite element (FE) model of a biomechanical system comprises of the various steps of geometrical discretization using viable meshing techniques, assignment of appropriate boundary conditions and loads, and the right interpretation of results, which are clinically relevant [44,45]. For our work, a non-linear transient FE analysis capturing the various phases (or time frames) of blast loading was adopted.

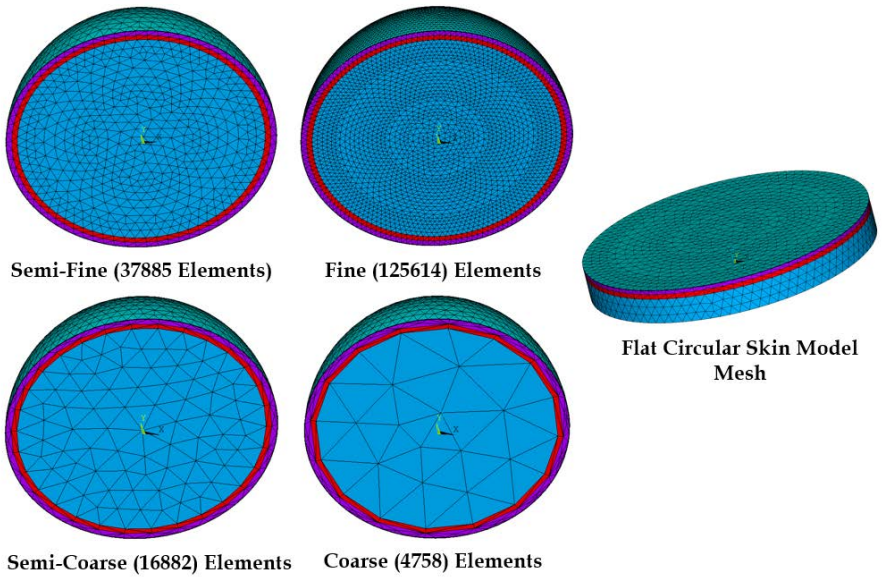

(A)

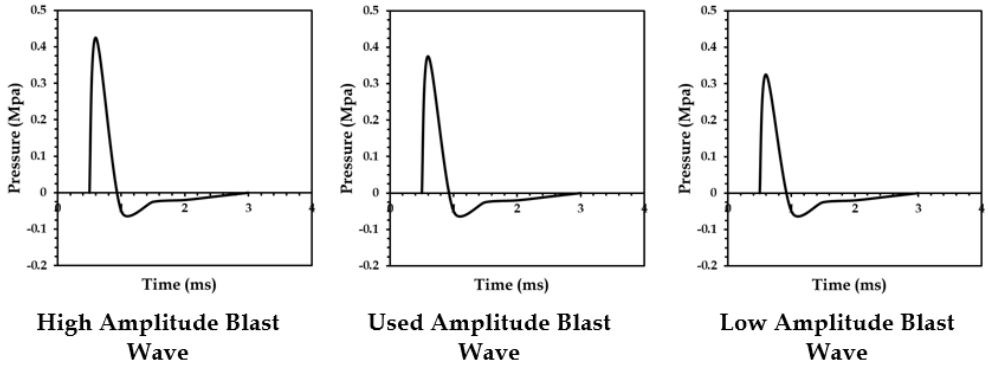

(B)

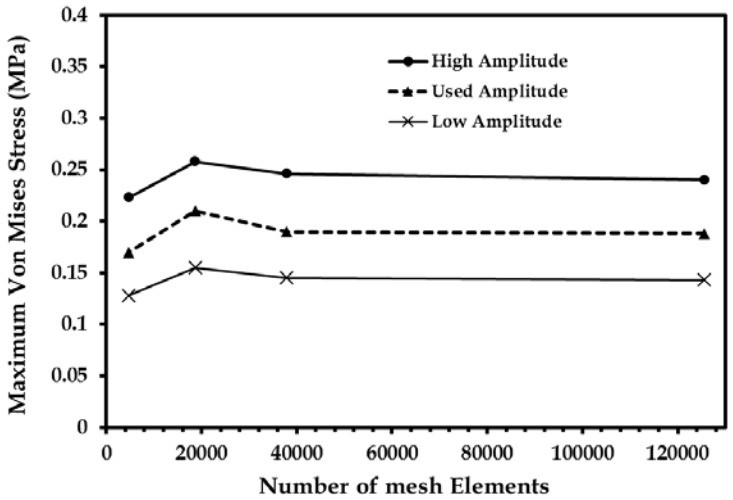

(C)

Figure 3. A) Meshes of a typical curved skin and bone section model for mesh convergence (MC) study, and flat circular model B) Blasts waves of varying amplitudes used in MC study, C) MC study results.

Higher order 3D 20-node Solid 186 type quadratic tetrahedral elements were chosen for meshing of all the skin and bone section layers. A detailed mesh convergence study was conducted to ensure accuracy of results from our analyses. Figure 3A shows the four meshes namely a coarse, semi-coarse, fine and very fine, which were subjected to blast loadings with three different amplitudes as shown in Figure 3B. Figure 3C presents the results of the mesh convergence study, from which, it was concluded that semi-fine mesh for the curved section with 37885 elements was a stable mesh for our further analyses. Appropriate mesh sizing controls (with a global element edge length of 0.1 mm was applied on the epidermal layer to obtain the semi-fine mesh in Figure 3A, followed by a continuum mesh generation for the dermis, hypodermis and the bone section in order) were used to ensure a smooth mesh transition from one layer to another, and also to optimize the number of elements generated [45]. For the current analyses, the bottom surface of the bone and skin layers were constrained in all degrees of freedom to simulate the strong attachment of the skin layers to the bone [46]. The constraints for a typical flat circular section and curved section models are shown in Figure 4A.

Blast loading (pressure) was applied to the flat circular and curved skin and bone section models as shown in Figure 4B with red contour lines. The blast load steps were characterized using the Friedlander equation 1, where P_s is the peak pressure and t^* is the time at which the pressure crosses the horizontal X axis for the first time (before the negative phase). Assuming P_s as 0.375 MPa from 0.5 to 0.6 ms, and −0.5 MPa from 0.6 to 1 ms, a t^* value of 0.826 ms was estimated numerically. Table 2 lists the four load steps applied sequentially to simulate the Friedlander blast wave in our analyses.

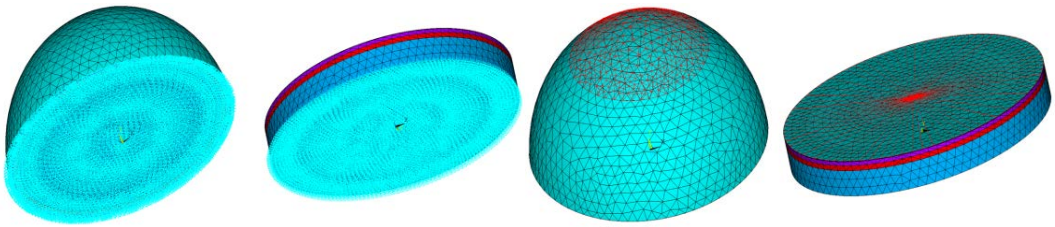

(A) **(B)**

Figure 4. A) Displacement constraints and B) Blast pressure applied (indicated by red contours), on the flat circular and curved section skin and bone computational models.

Table 2. Pressure loads applied at different times (load steps) to simulate blast loading [2] in our computational models.

Load Step	Time (ms)	Load/Pressure (MPa)
1	0–0.5	0
2	0.5–0.6	0.375
3	0.6–1	−0.05
4	1–3	0

$$P(t) = P_S\, e^{-\frac{t}{t^*}}\left[1-\frac{t}{t^*}\right] \quad (1)$$

Regarding the boundary conditions employed in our work (Figure 4), it should be mentioned that a pressure-time history usually doesn't apply directly on a structure in a blast scenario. However, under the assumption of close proximity of a subject to the blast and the consequent incidence of an uniform blast pressure from all directions, such an application of a time varying pressure on a model directly is reasonable. Additionally, a sudden change in the moment of inertia (or motions) of skin (over less than a millisecond) with respect to a relatively stationary bone structure of an individual has been assumed to reasonably constrain the bottom of the bone section in all degrees of freedom.

Soft tissues like skin show non-linear viscoelastic behavior under tension or compression. Hyperelastic curve fit equations such as Mooney-Rivlin, Neo-Hookean, Martins and Yeoh can be used to characterize soft tissue behavior precisely [47]. Equation 2 shows the Yeoh's hyperelastic constitutive equation relating the stress (σ) and the stretch ($\lambda = 1+\varepsilon$), for uniaxial and isotropic mechanical test. The parameters c_{10}, c_{20}, and c_{30} are the curve fit parameters, and I_1, I_2 and I_3 are the invariants of the Cauchy Green tensor [47], and also functions of the Principal Stretches (λ_i, I = 1,2 and 3) along the X, Y, and Z Cartesian coordinate directions, as given by equations 3-5. The parameter d_i used in equation 6 is mainly for FEM calculations in ANSYS. K is bulk modulus in equation 6.

$$\sigma_{Yeoh} = 2(\lambda_i^{\,2} - \frac{1}{\lambda_i})(c_{10} + 2c_{20}(I_1 - 3) + 3c_{30}(I_1 - 3)^2), i = 1 \tag{2}$$

$$I_1 = \sum_{i=1}^{3} \lambda_i^2 \tag{3}$$

$$I_2 = \sum_{i,\,j=1}^{3} \lambda_i^2 \lambda_j^2, i \neq j \tag{4}$$

$$I_3 = \prod_{i=1}^{3} \lambda_i^2 \tag{5}$$

$$d_i = \frac{2}{K} \tag{6}$$

In the current work, based on the literature on the mechanical testing of the dermis [48], Yeoh's model parameters were determined (listed in Table 3) using curve fitting techniques. The reason why Yeoh's model was chosen specifically over any other non-linear material model was because it has been used recently to accurately predict the mechanical properties of the skin [49], brain [50] and breast tissues [51].

The epidermal mechanical properties of the Caucasian skin (Subject 1) was obtained (listed in Table 3) from the literature [52]. Also, in literature, the elasticity of the epidermal skin layer was reported to be about 26% higher for an African-American person compared to a Caucasian person [53–56]. The reason behind such a variation was found to be because of the amount of melanin (the pigment which gives human skin their color) content in the skin. As the skin color for Asian skin (subjects 2 and 3) would lie between that of Caucasian and African-American skin, a 5% and 15% higher modulus of elasticity was assumed for the subject 2 and subject 3 respectively, compared to in the case of Subject 1 [53–56] (listed in Table 3). Linear elastic mechanical properties were adopted for the hypodermis (muscles) and bone section [27], which are also listed in Table 3. The reason behind choosing a linear material model for the epidermis and hypodermis was mainly

the non-availability of non-linear experimental studies unlike in case of the dermis. Such a partly non-linear model is an improvement over most of the completely linear material models adopted in literature for skin related computational studies.

Table 3. Material model parameters adopted for the skin and bone computational models.

Non-Linear Material Property for Dermis				
Yeoh Model Parameters	C_{10} (MPa)	C_{20} (MPa)	C_{30} (MPa)	d_1, d_2 and d_3
Subject 1, 2 and 3	0.948	4.946	0.01	0.222
Linear Material Properties for Epidermis				
Linear Elastic Parameters	Modulus of Elasticity (MPa)	Poisson's Ratio		
Subject 1	5.0	0.46		
Subject 2	5.25	0.45		
Subject 3	5.75	0.47		
Linear Material Properties for Hypodermis/Muscles				
Linear Elastic Parameters	Modulus of Elasticity (MPa)	Poisson's Ratio		
Subject 1, 2 and 3	100	0.45		
Linear Material Properties for Bone Section				
Linear Elastic Parameters	Modulus of Elasticity (MPa)	Poisson's Ratio		
Subject 1, 2 and 3	15000	0.23		

3. Results and Discussions

The average von Mises stress profiles observed typically at the flat circular and curved skin and bone section models were captured. Figure 5 shows the effect of the applied blast load observed on the entire bone and the skin section model for load step 2 (peak pressure), for one of the flat circular (forehead) and curved (wrist) models. Figure 6 captures the same, but for the load step 3 (negative pressure).

To further study the effect of blast on the bone section and the various skin layers, the stresses at each of these layers were quantified numerically over time. The following sections present the snapshots and plots for the same.

Besides studying whole body injury computationally, the current work can be extended to study blast-induced traumatic brain injury (TBI) by measurement of the subject-specific curvature of the skull and by incorporating the skin layer thicknesses and material properties from literature.

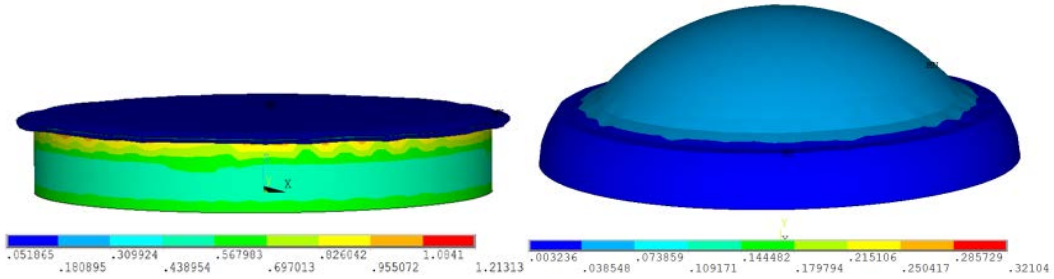

(A) **(B)**

Figure 5. Blast loading effects at load step 2 (peak pressure) for computational models of A) Forehead of subject 3, and B) Wrist of subject 2.

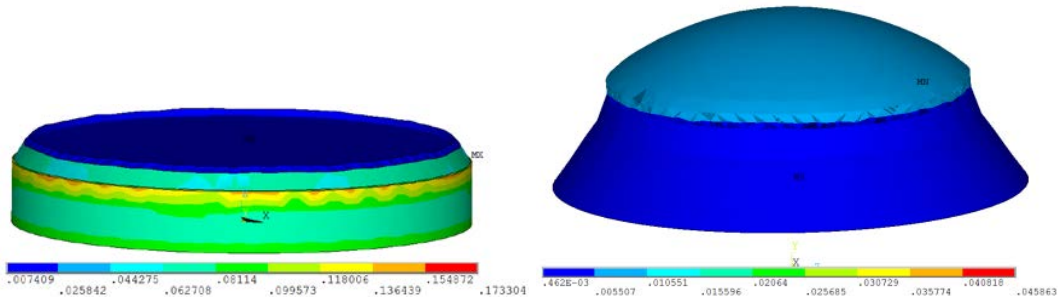

(A) **(B)**

Figure 6. Blast loading effects at load step 3 (negative pressure) for computational models of A) Forehead of subject 3, and B) Wrist of subject 2.

3.1. Bone Stresses

The average stresses on the bone section were estimated over time. Figure 7 captures the stress profile of the bone sections for a flat circular (forehead) and curved (wrist) model at load step 2 (peak pressure). Higher maximum stresses were observed for the flat circular bone section compared to the curved bone section. Also the maximum bone stress developed at the flat circular bone section (1.21 MPa) and curved bone section (0.427 MPa) were greater than the applied blast peak pressure (0.375 MPa), which can be seen in Figure 7B. It can be concluded that flat circular bone sections (like forehead and shin) are much more vulnerable to blast stresses (and consequent fracture) than curved bone sections (such as fingers, wrists and elbow).

At load step 3 (negative pressure), the stresses observed at the flat circular bone section was higher than at the curved bone section (see Figure 8). Also, the maximum bone stress observed at both the flat circular bone section (0.173 MPa) and curved bone section (0.061 MPa) were much higher than the negative pressure (−0.05 MPa) applied at load step 3. It can be concluded that the flat circular bone sections are much more prone to blast damage due to negative pressure compared to curved bone sections.

Stress versus time has been plotted for the bone sections in all subject-specific computational models (See Figure 9). The main observations are: 1) The peak stress values are higher in flat circular skin and bone models compared to the curved ones, 2) For the curved models (mainly in the

forehead), the subject-specific variations in bone stresses are minimal. This could be attributed to the minimal "thickness" changes in skin and bone layers in forehead, which may be an important regulator of stress than the subject-specific variation due to material properties.

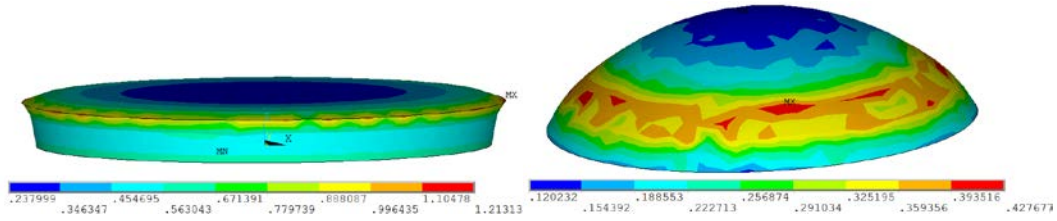

(A) **(B)**

Figure 7. Blast loading effects at load step 2 (peak pressure) for bone section of A) Forehead of subject 3, and B) Wrist of subject 2.

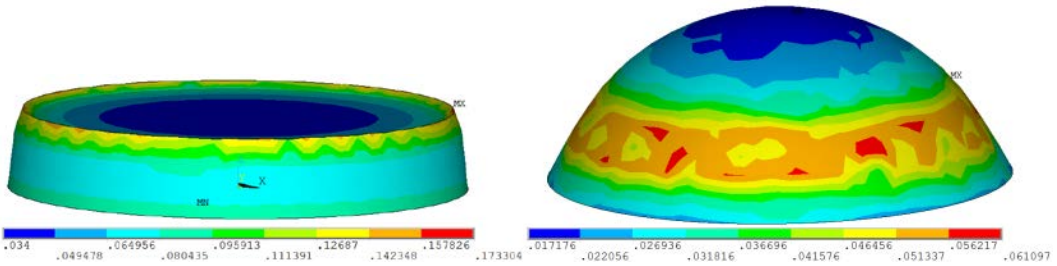

(A) **(B)**

Figure 8. Blast loading effects at load step 3 (negative pressure) for bone section of A) Forehead of subject 3, and B) Wrist of subject 2.

3.2. Hypodermal (muscle) stresses

Blast-induced hypodermal (muscle) stresses are captured for a flat circular section (forehead) and curved section (wrist) skin and bone models. The flat circular model looks thin as the hypodermal (or muscle) layer is very thin on the forehead. The maximum stress for the flat circular section (0.93 MPa) was observed to be higher than the peak blast pressure (0.375 MPa) applied at the load step 2. Compared to the maximum bone stresses discussed in the previous section, the hypodermal stresses were found to be lower in average. Also, the stress distribution was found to be much more uniform in Figure 10 for the curved hypodermal section compared to the curved bone section (discussed earlier in Figure 7B). There were no sudden maximum stress build-ups (in Figure 10 B) unlike in bone section in Figure 7 B.

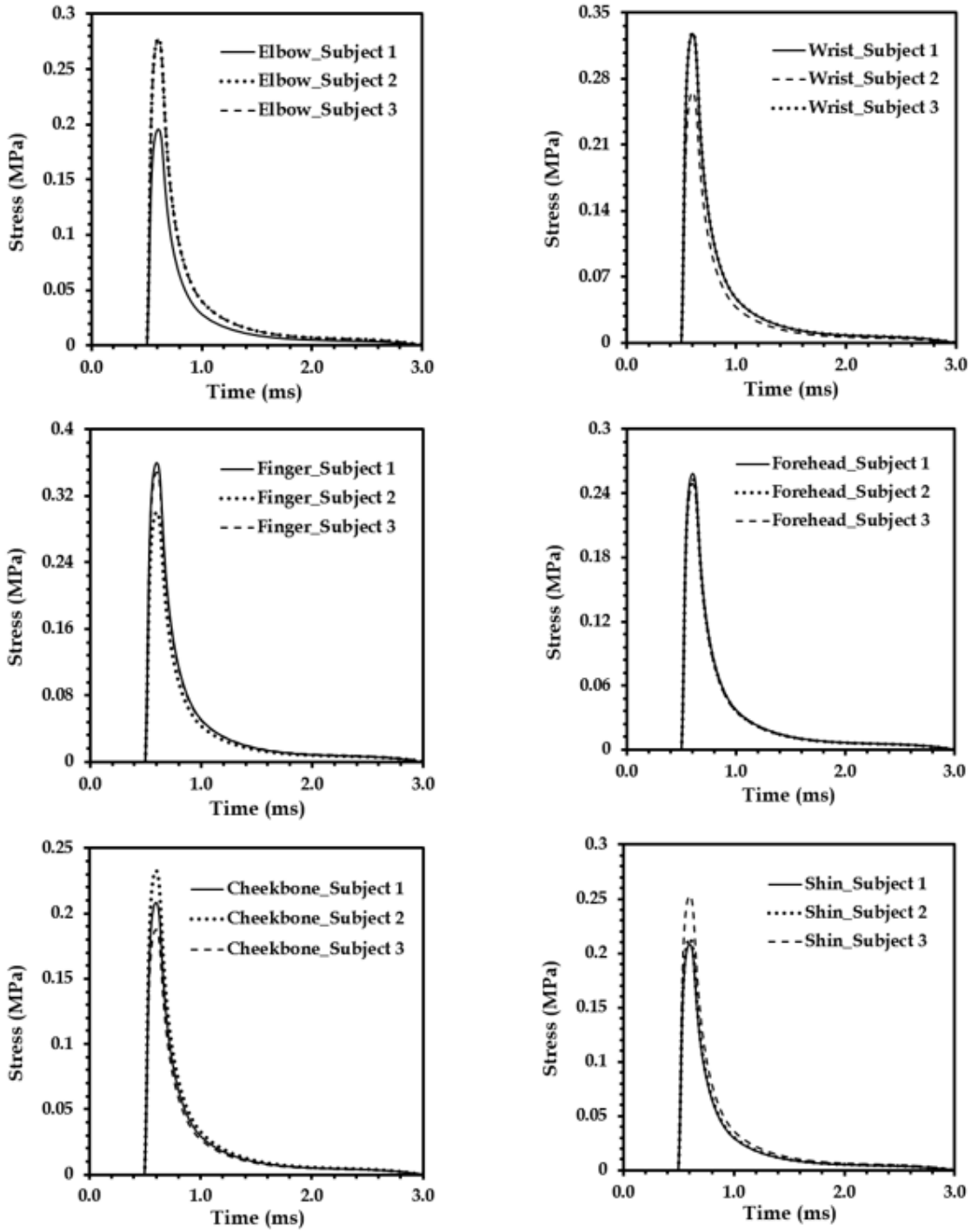

Figure 9. Subject-Specific bone stresses over time for various skin and bone models.

At load step 3 (see Figure 11), the maximum stress at the curved surface (0.03 MPa) was found to be less than the applied negative blast pressure (−0.05 MPa). However, for the flat circular section, the maximum stress developed (0.132 MPa) was found to be higher than the applied negative blast pressure.

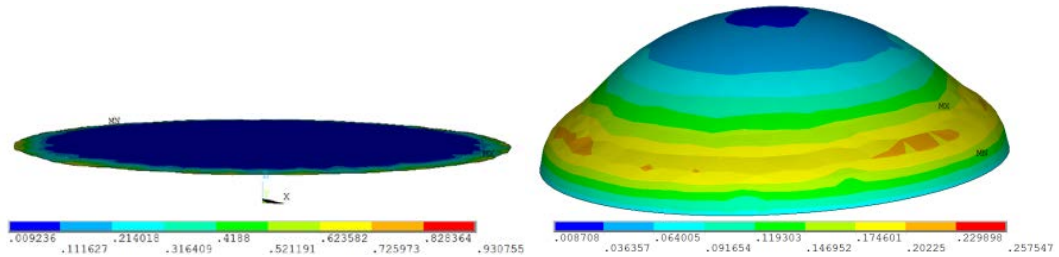

(A) **(B)**

Figure 10. Blast loading effects at load step 2 (peak pressure) for hypodermal skin layer of A) Forehead of subject 3, and B) Wrist of subject 2.

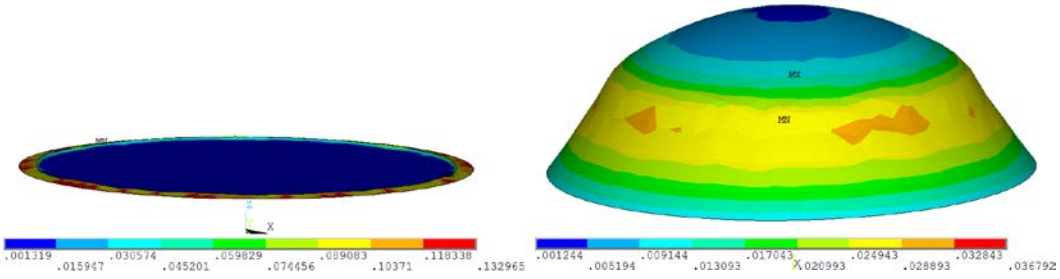

(A) **(B)**

Figure 11. Blast loading effects at load step 3 (negative pressure) for hypodermal skin layer of A) Forehead of subject 3, and B) Wrist of subject 2.

From the stress versus time plots at the hypodermal (muscle) sections of the subject-specific computational models (see Figure 12), minimal variations in the stress versus time profile were observed among the three subjects in the case of forehead, shin, and also elbow. However, for the wrist, cheekbone and the finger sections, huge subject-specific variations were observed. This finding could be mainly attributed to the minimal thickness of the hypodermal (muscle) section at the elbow, forehead and the shin, compared to a reasonable muscle thickness at the wrist, cheekbone and the finger sections. Additionally for finger and wrist hypodermal sections, the subject 3 was found to experience the maximum peak stresses at both the load steps 2 and 3. The main reason behind this observation was found to be the geometrical thickness differences among the subjects. Also an inferior dependence on the subject-specific epidermal material property (see Table 3) was observed.

In subject 3, for the case of the cheekbone, the hypodermal stress peak at load steps 2 and 3 were observed to be the minimum. On further investigation, the subject-specific geometrical difference was found to be the major reason behind the finding, with an inferior effect of the subject-specific material property variations, which needs further investigation in the future.

3.3. Dermal stresses

Dermis is the thickest layer of skin where the blood vessels end. Thus any bleeding due to injury such as in blasts could be mainly attributed to the rupture of the dermis. Figure 13 captures the effect of blast peak pressure at load step 2 on a flat circular dermal section (from the forehead) and a curved section (from the wrist). The maximum stress at the flat circular dermis section (0.49 MPa) in

Figure 13 A was found to be greater than the applied peak blast pressure (0.375 MPa) at load step 2. However for the curved dermis section, the maximum stress was lower than the peak blast pressure.

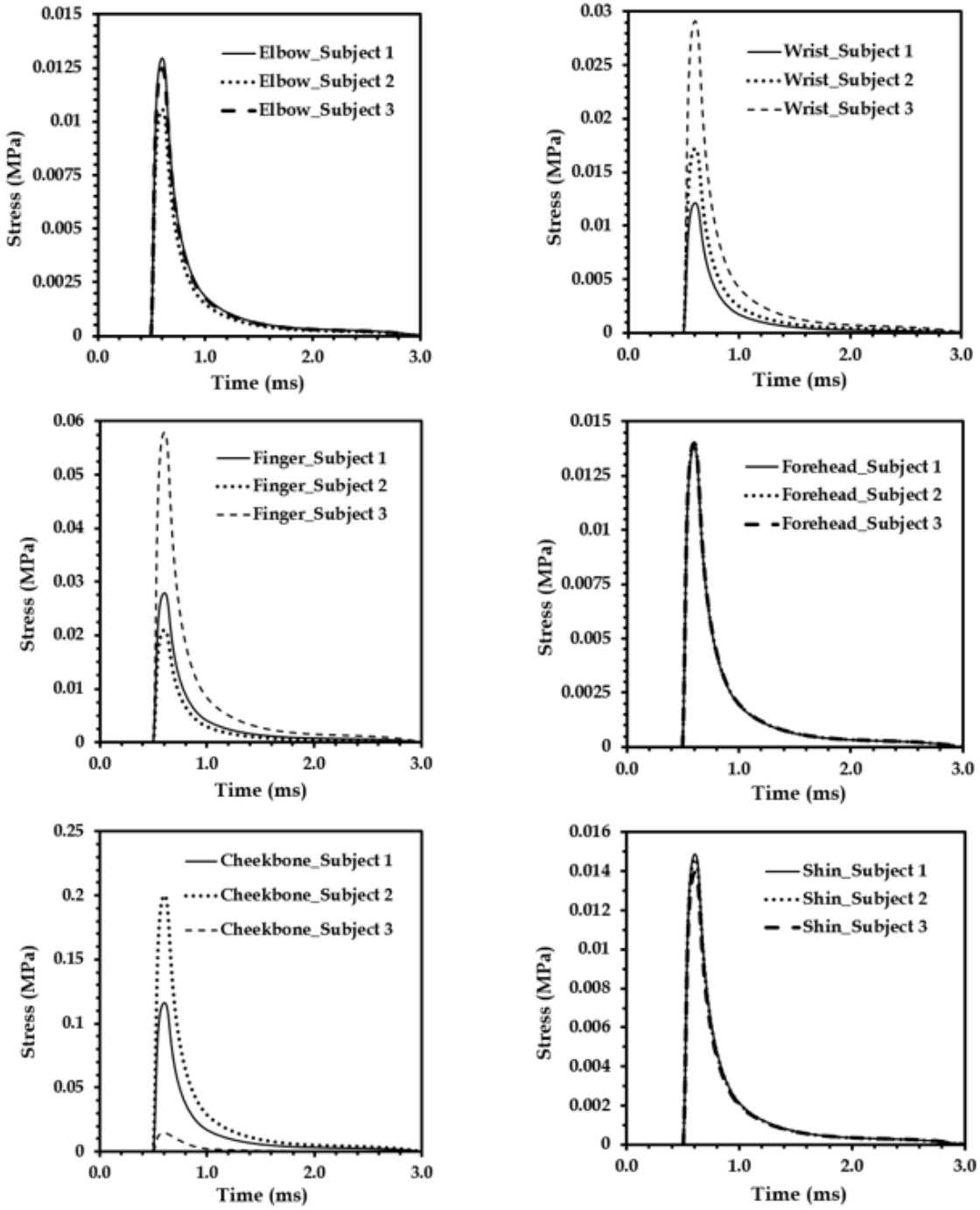

Figure 12. Subject-Specific hypodermal (muscle) stresses over time for various skin and bone models.

A similar finding was observed in case of load step 3 (negative blast pressure), where the applied negative blast pressure was less than the maximum stress at the flat circular dermal section, but greater than the maximum stress at the curved dermal section (See Figure 14). It was concluded that: 1) The curvature of the skin and bone section model indeed reduces the stress at each of the skin

and bone sections, and 2) For soft materials such as the skin layers and muscles, the stress has a tendency to go below the applied blast pressure both at the peak and trough (negative pressure state).

From the blast-induced subject-specific stress versus time plots of the dermis (see Figure 15), a minimal change in the stress-time profile was observed for the elbow, forehead, and also the shin sections. This finding may be attributed to the extremely thin dermal layers present in all these locations. For the wrist, finger and cheekbone sections, reasonable subject-specific variations were observed in the dermal stresses with time, which however were found to be more of a sectional geometry effect than the effect of varying skin material properties.

In case of the cheekbone, similar to what was observed in the previous section, the huge variation in subject-specific dermal stresses were found (see Figure 15) to be due to the high sensitivity of the stresses in relation to the sectional geometrical parameters. Also, the variations in the subject-specific epidermal material properties were confirmed from our simulations to have an inferior effect on the stresses. The cheekbone section may be studied in the future specifically for further investigating the observed subject-specific trends.

The material behavior exhibited by the dermal skin layer in our analysis was validated extensively during our study on fabrication and manufacturing of skin simulants from various locations on the human body. This novel experimental work by Chanda and Unnikrishnan et al. has been applied for a patent [49] in the U.S. recently.

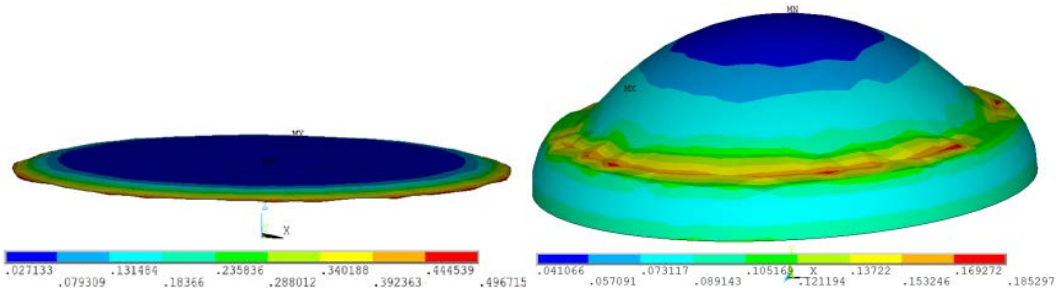

(A) **(B)**

Figure 13. Blast loading effects at load step 2 (peak pressure) for dermal skin layer of A) Forehead of subject 3, and B) Wrist of subject 2.

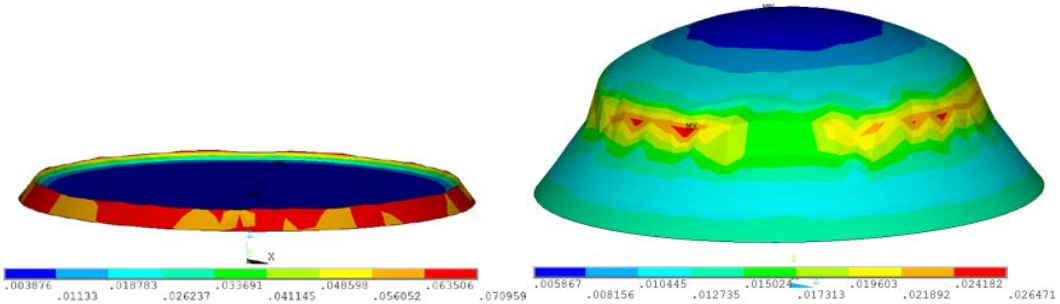

(A) **(B)**

Figure 14. Blast loading effects at load step 3 (negative pressure) for dermal skin layer of A) Forehead of subject 3, and B) Wrist of subject 2.

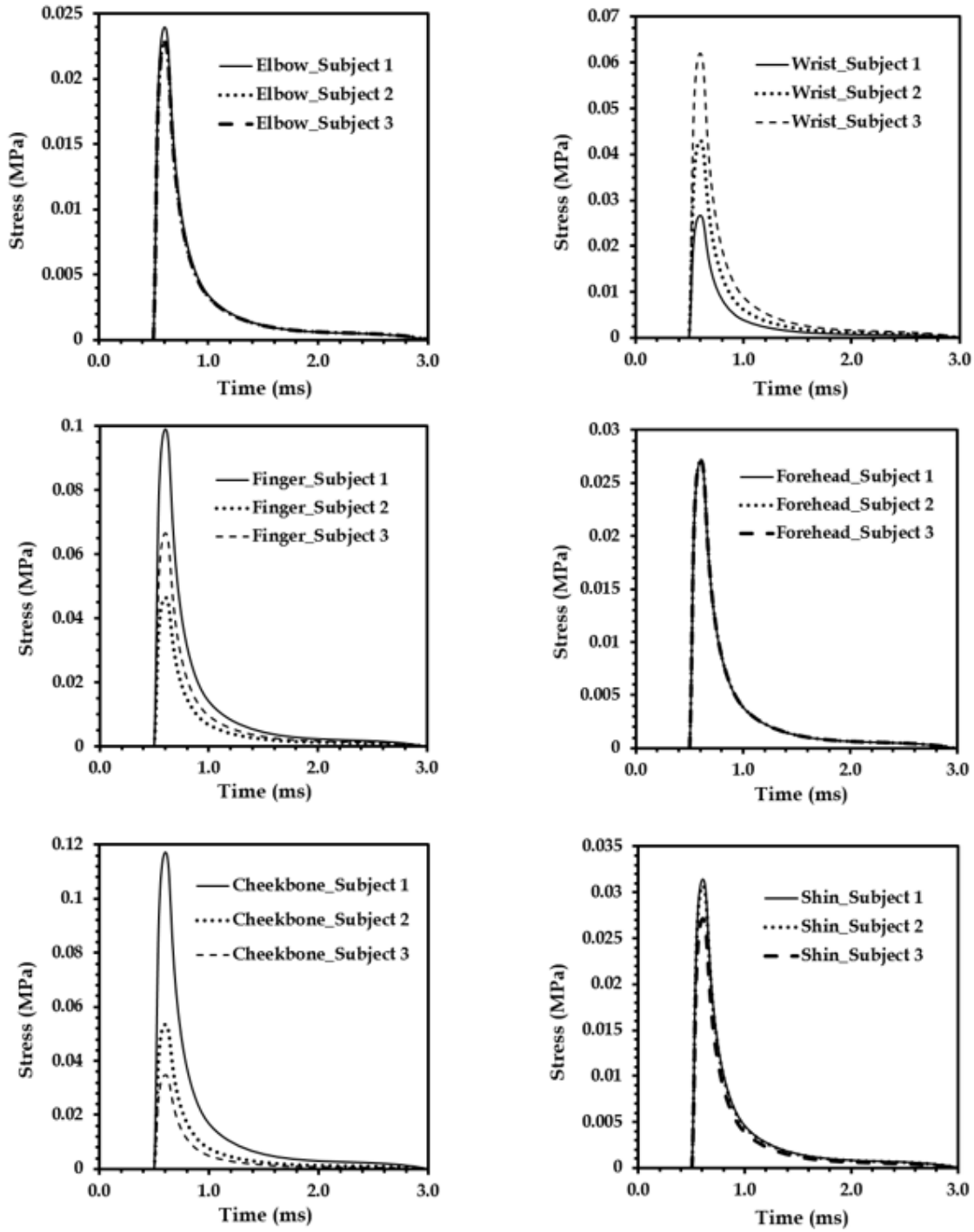

Figure 15. Subject-Specific dermal stresses over time for various skin and bone models.

3.4. Epidermal stresses

Epidermis, which is the outermost layer of the skin, and the most elastic (or weak) was found to develop low stresses compared to the applied blast pressures for both load step 2 (peak pressure condition, shown in Figure 16) and 3 (negative pressure condition, shown in Figure 17). The stress reduction effect of the curvature was also observed with the epidermal section, like we saw with the dermis, hypodermis and the bone section in earlier sections. Figure 18 presents the stress versus time variations in epidermis of the various subject-specific skin and bone models. Like in case of dermis (discussed in section 3.3), minimal variations were observed in the stress versus time plots of the elbow, forehead, and shin. Also, for the wrist and finger, a limited subject-specific variation in the epidermal stress profile was observed over time. These observations may be because of the very small thickness of the epidermal layer in all body locations and subjects. The cheekbone epidermal section however showed significant subject-specific variations in the stress profiles. The reason behind this trend with the cheekbone is consistent with the trends observed earlier in case of the dermis, hypodermis and the bone section, due to a high influence of geometrical variations and an inferior effect of material property variations.

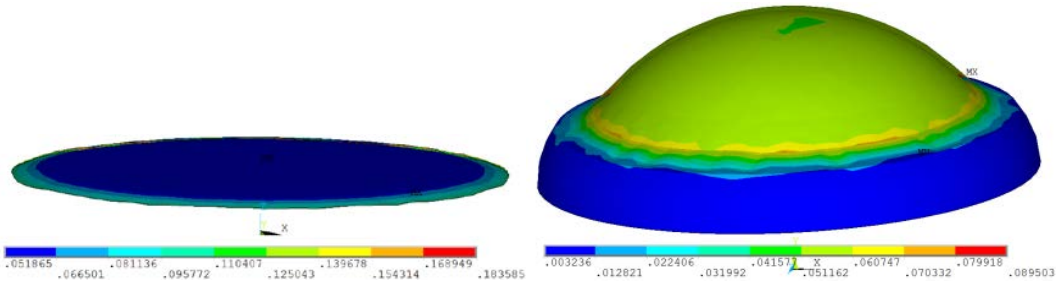

(A) **(B)**

Figure 16. Blast loading effects at load step 2 (peak pressure) for epidermal skin layer of A) Forehead of subject 3, and B) Wrist of subject 2.

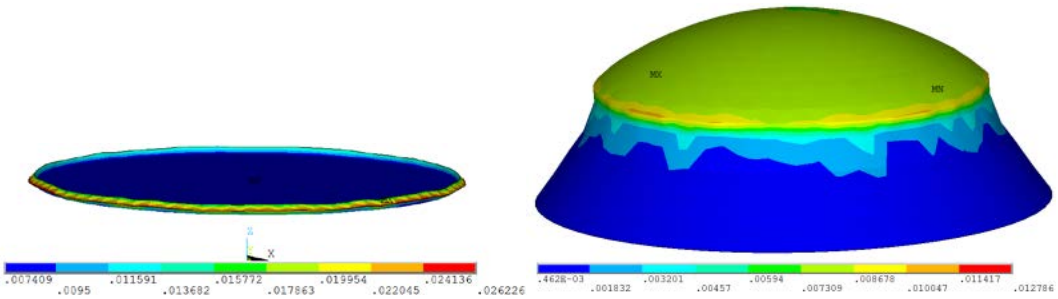

(A) **(B)**

Figure 17. Blast loading effects at load step 3 (negative pressure) for epidermal skin layer of A) Forehead of subject 3, and B) Wrist of subject 2.

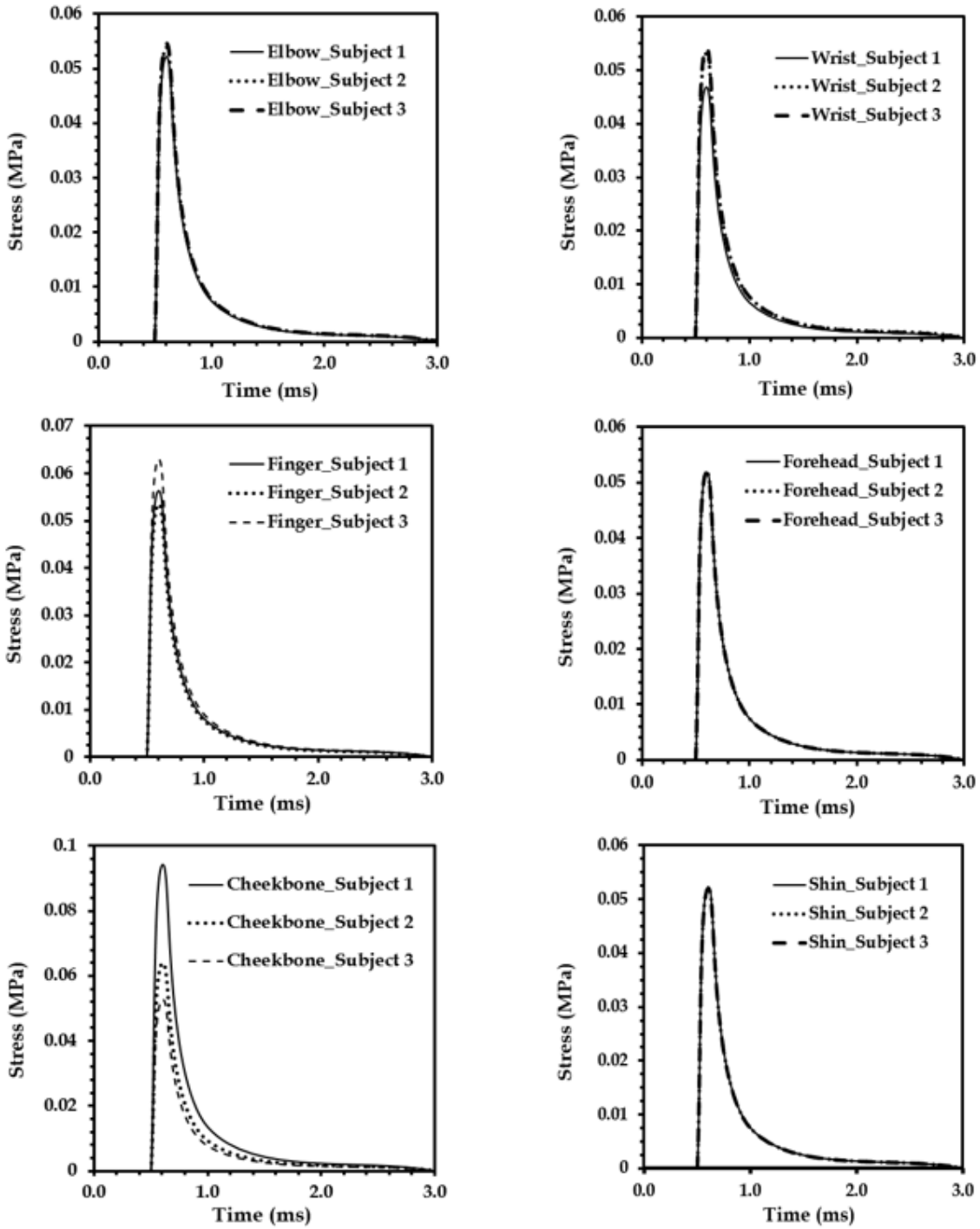

Figure 18. Subject-Specific epidermal stresses over time for various skin and bone models.

4. Conclusions

In this current work, subject-specific computational models of the skin and bone layers from six different sections of the human body (forehead, finger, wrist, shin, elbow and cheekbone) were modelled using Finite Element Method (FEM). All the models were subjected to a dynamic primary blast loading, and the stresses at each skin and bone layers were estimated quantitatively.

Table 4. Summary of results observed in the skin and bone sections under the influence of the blast loading.

Layer Studied	Major Findings
Bone Section	-Maximum bone stress developed at the flat circular bone section (1.21 MPa) and curved bone section (0.427 MPa) were greater than the applied blast peak pressure (0.375 MPa) -Flat circular bone sections (like forehead and shin) are much more vulnerable to blast stresses (and consequent fracture) than curved bone sections (such as fingers, wrists and elbow) -At the forehead, the subject-specific variations in bone stresses are minimal
Hypodermis (Muscles)	-The maximum stress for the flat circular section (0.93 MPa) was higher than the peak blast pressure (0.375 MPa) -Hypodermal stresses were lower than bone stresses -Curved hypodermal sections had more uniform stress distribution compared to curved bone sections -Minimal subject-specific variations in the case of forehead, shin, and elbow -Maximum peak stresses (at finger and wrist) and minimal peak stresses (at cheekbone) observed for Subject 3
Dermis	-Lower peak stresses compared to the bone and hypodermis -The maximum stress at the flat circular dermis section (0.49 MPa) was greater than the applied peak blast pressure (0.375 MPa) -The cheekbone stresses were high sensitivity to subject-specific variations
Epidermis	-Lowest peak stresses compared to other sections -Due to minimal thickness, low sensitivity to subject-specific variations -Stresses were more influenced by geometrical variations compared to material property differences

Some of the major findings from these analyses were: 1) The stresses developed on the skin and the bone significantly depends on the geometry of the section of the human body exposed to a blast wave, 2) Curvature in general greatly reduces the blast stresses developed in the skin and bone layers. However, the actual relation between curvature and blast induced stresses is unknown and would be a subject of future studies, 3) The highest amount of stresses due to blasts are developed in the bone, followed by the hypodermis, dermis, and the epidermis, 4) Subject-specific variations in stresses developed in the skin and bone layers over time were mainly observed due to sectional geometry effects (especially curvature and layer thicknesses) and minimally due to differences in material properties, 5) Minimal subject-specific variations were observed in the stresses developed in the skin layers of the forehead, elbow and shin, as the skin and muscle layers are extremely thin in these regions. Other subject-specific trends were identified for stresses developed in the skin and bone layers (summarized in Table 4), which needs further parametric investigation in the future.

To date, this blast-induced subject and location specific skin and bone section study is the first of its kind ever attempted. The results of this investigation would be indispensable for: 1) Understanding the biomechanics of the skin and bone sections from various locations of the human body under blast loading, the knowledge of which could be very helpful for doctors and medical

practitioners to estimate post-blast trauma and devise effective mitigation strategies accordingly, 2) Understanding subject-specific trends of blast-induced skin and bone injury and trauma, and 3) For designing of better personal protection equipment (PPE) for blast mitigation at different locations of the human body.

Acknowledgements

VU would like to acknowledge the faculty start-up funds, and the 2014 RGC seed grants from The University of Alabama (UA).

Conflict of Interest

All authors declare no conflicts of interest in this paper.

References

1. Kulkarni S, Gao X-L, Horner S, et al. (2013) Ballistic helmets-Their design, materials, and performance against traumatic brain injury. *Compos Struct* 101: 313–331.
2. Jenson D, Unnikrishnan VU (2015) Energy dissipation of nanocomposite based helmets for blast-induced traumatic brain injury mitigation. *Compos Struct* 121: 211–216.
3. Stuhmiller JH, Phillips Y, Richmond D (1991) The physics and mechanisms of primary blast injury. *Conventional warfare: ballistic, blast, and burn injuries Washington, DC: Office of the Surgeon General of the US Army*, 241–270.
4. Born CT (2004) Blast trauma: the fourth weapon of mass destruction. *Scandinavian journal of surgery: SJS: official organ for the Finnish Surgical Society and the Scandinavian Surgical Society* 94: 279–285.
5. Chandra N, Ganpule S, Kleinschmit N, et al. (2012) Evolution of blast wave profiles in simulated air blasts: experiment and computational modeling. *Shock Waves* 22: 403–415.
6. Chandra N, Skotak M, Wang F, et al. (2013) Do Primary Blast-Shock Waves Cause Mild TBI? Experimental Evidence Based On Animal Models And Human Cadaveric Heads. Mary Ann Liebert, Inc 140 Huguenot Street, 3rd Fl, New Rochelle, NY 10801 USA, A80–A80.
7. Ganpule SG, Chandra N, Salzar R (2013) Mechanics Of Blast Loading On Post-Mortem Human Heads in The Study Of Traumatic Brain Injury (TBI) Using Experimental And Computational Approaches [PhD Dissertation]: University of Nebraska-Lincoln, 289.
8. Ganpule S, Chandra N (2013) Mechanics of Interaction of Blast Waves on Surrogate Head: Effect of Head Orientation. ASME 2013 Summer Bioengineering Conference: American Society of Mechanical Engineers, V01BT55A028-029.
9. Kangarlou K (2013) Mechanics of Blast Loading on the Head Models in the Study of Traumatic Brain Injury. *Nationalpark-Forschung In Der Schweiz (Switzerland Research Park Journal)*, 102.
10. Sundaramurthy A, Alai A, Ganpule S, et al. (2012) Blast-induced biomechanical loading of the rat: an experimental and anatomically accurate computational blast injury model. *J Neurotraum* 29: 2352–2364.
11. Chafi MS, Ganpule S, Gu L, et al. (2011) Dynamic response of brain subjected to blast loadings: influence of frequency ranges. *Int J Appl Mech* 3: 803–823.

12. Ganpule S, Gu L, Alai A, et al. (2012) Role of helmet in the mechanics of shock wave propagation under blast loading conditions. *Computer Methods Biomec* 15: 1233–1244.
13. Ganpule S, Gu L, Cao G, et al. (2009) The effect of shock wave on a human head. ASME 2009 International Mechanical Engineering Congress and Exposition: American Society of Mechanical Engineers, 339–346.
14. Ganpule S, Gu L, Chandra N (2010) MRI-based three dimensional modeling of blast traumatic brain injury (bTBI). ASME 2010 International Mechanical Engineering Congress and Exposition: American Society of Mechanical Engineers, 181–183.
15. Gu L, Chafi MS, Ganpule S, et al. (2012) The influence of heterogeneous meninges on the brain mechanics under primary blast loading. *Compos Part B-Eng* 43: 3160–3166.
16. Gupta RK, Przekwas A (2013) Mathematical models of blast-induced TBI: current status, challenges, and prospects. *Front Neurol* 4: 59.
17. Hayda R, Harris RM, Bass CD (2004) Blast injury research: modeling injury effects of landmines, bullets, and bombs. *Clin Orthop Relate R* 422: 97–108.
18. Jenson D, Unnikrishnan V (2014) Multiscale Simulation of Ballistic Composites for Blast Induced Traumatic Brain Injury Mitigation. ASME 2014 International Mechanical Engineering Congress and Exposition: American Society of Mechanical Engineers. V009T012A072–V009T012A077.
19. Hull J (1992) Traumatic amputation by explosive blast: pattern of injury in survivors. *Brit J Surg* 79: 1303–1306.
20. DePalma RG, Burris DG, Champion HR, et al. (2005) Blast injuries. *New Engl J Med* 352: 1335–1342.
21. Wightman JM, Gladish SL (2001) Explosions and blast injuries. *Ann Emerg Med* 37: 664–678.
22. Gondusky JS, Reiter MP (2005) Protecting military convoys in Iraq: an examination of battle injuries sustained by a mechanized battalion during Operation Iraqi Freedom II. *Mil Med* 170: 546.
23. Beekley AC, Blackbourne LH, Sebesta JA, et al. (2008) Selective nonoperative management of penetrating torso injury from combat fragmentation wounds. *J Trauma Acute Care* 64: S108–S117.
24. Xydakis MS, Fravell MD, Nasser KE, et al. (2005) Analysis of battlefield head and neck injuries in Iraq and Afghanistan. *Otolaryng Head Neck* 133: 497–504.
25. Breeze J, Allanson-Bailey LS, Hunt NC, et al. (2012) Mortality and morbidity from combat neck injury. *J Trauma Acute Care* 72: 969–974.
26. Dussault MC (2013) Blast injury to the human skeleton: recognition, identification and differentiation using morphological and statistical approaches [PhD dissertation]: Bournemouth University, School of Applied Sciences, 350.
27. Bertucci R, Liao J, Williams L (2011) Development of a Lower Extremity Model for Finite Element Analysis at Blast Condition. ASME 2011 Summer Bioengineering Conference: American Society of Mechanical Engineers, 1035–1036.
28. Netter FH (2014) Atlas of human anatomy. Philadelphia, PA: Elsevier Health Sciences.
29. Wolpoff MH, Caspari R (1997) *Race and human evolution*. New York, NY: Simon and Schuster.
30. Barker DE (1951) Skin thickness in the human. *Plast Reconstr Surg* 7: 115–116.
31. Domaracki M, Stephan CN (2006) Facial Soft Tissue Thicknesses in Australian Adult Cadavers*. *J Forensic Sci* 51: 5–10.

32. Fields ML, Greenberg BH, Burkett LL (1967) Roentgenographic measurement of skin and heel-pad thickness in the diagnosis of acromegaly. *Am J Med Sci* 254: 528–533.
33. Garn SM, Haskell JA (1960) Fat thickness and developmental status in childhood and adolescence. *AM J Dis Child* 99: 746–751.
34. Holbrook KA, Odland GF (1974) Regional differences in the thickness (cell layers) of the human stratum corneum: an ultrastructural analysis. *J Invest Dermatol* 62: 415–422.
35. Hwang HS, Park MK, Lee WJ, et al. (2012) Facial soft tissue thickness database for craniofacial reconstruction in Korean adults. *J Forensic Sci* 57: 1442–1447.
36. Lee Y, Hwang K (2002) Skin thickness of Korean adults. *Surg Radiol Anat* 24: 183–189.
37. Sahni D, Singh G, Jit I, et al. (2008) Facial soft tissue thickness in northwest Indian adults. *Forensic Sci Int* 176: 137–146.
38. Simpson E, Henneberg M (2002) Variation in soft tissue thicknesses on the human face and their relation to craniometric dimensions. *Am J Phys Anthropol* 118: 121–133.
39. Sipahioğlu S, Ulubay H, Diren HB (2012) Midline facial soft tissue thickness database of Turkish population: MRI study. *Forensic Sci Int* 219, 1–282: e1–e8.
40. Southwood W (1955) The thickness of the skin. *Plast Reconstr Surg* 15: 423–429.
41. Tedeschi-Oliveira SV, Melani RFH, de Almeida NH, et al. (2009) Facial soft tissue thickness of Brazilian adults. *Forensic Sci Int* 193, 1-127: e1–e7.
42. Whitmore SE, Sago NJG (2000) Caliper-measured skin thickness is similar in white and black women. *J Am Acad Dermatol* 42: 76–79.
43. Whitton JT (1973) New values for epidermal thickness and their importance. *Health Phys* 24: 1–8.
44. Chanda A, Unnikrishnan V, Roy S, et al. (2015) Computational Modeling of the Female Pelvic Support Structures and Organs to Understand the Mechanism of Pelvic Organ Prolapse: A Review. *Appl Mech Rev* 67: 040801.
45. Chanda A, Ghoneim H (2015) Pumping potential of a two-layer left-ventricle-like flexible-matrix-composite structure. *Compos Struct* 122: 570–575.
46. Gray H (1918) *Anatomy of the human body*. Baltimore, MD: Lea & Febiger.
47. Martins P, Natal Jorge R, Ferreira A (2006) A Comparative Study of Several Material Models for Prediction of Hyperelastic Properties: Application to Silicone Rubber and Soft Tissues. *Strain* 42: 135–147.
48. Annaidh AN, Bruyère K, Destrade M, et al. (2012) Characterization of the anisotropic mechanical properties of excised human skin. *J Mech Behav Biomed* 5: 139–148.
49. Chanda A, Unnikrishnan V, Flynn Z (2015) Biofidelic Human Skin Simulant. US Patent Application No 62/189, 504.
50. Kaster T, Sack I, Samani A (2011) Measurement of the hyperelastic properties of ex vivo brain tissue slices. *J Biomech* 44: 1158–1163.
51. O'Hagan JJ, Samani A (2009) Measurement of the hyperelastic properties of 44 pathological ex vivo breast tissue samples. *Phys Med Biol* 54: 2557.
52. Flynn CO (2007) The design and validation of a multi-layer model of human skin [PhD Dissertation]. Sligo, Ireland: Institute of Technology, Sligo.
53. Adegbenro A, Taylor S (2013) Structural, Physiological, Functional, and Cultural Differences in Skin of Color. *Skin of Color*: Springer, 1–19.

54. Saggar S, Wesley NO, Moulton-Levy NM, et al. (2007) *Ethnic differences in skin properties: the objective data*. Boca Raton, FL: Taylor & Francis.
55. Wesley NO, Maibach HI (2003) Racial (ethnic) differences in skin properties. *Am J Clin Dermatol* 4: 843–860.
56. Yosipovitch G, Theng C (2002) Asian skin: its architecture, function and differences from Caucasian skin. *Cosmetics Toiletries* 117: 57–62.

AIMS Press